CHROMOSOME PACKING IN CELL NUCLEI: TOWARDS UNDERSTANDING OF RADIATION-INDUCED GENE TRANSLOCATION FREQUENCY

Joanna Deperas-Standyło, Michał Cieśla

Institute of Theoretical Physics, Jagiellonian University
Łojasiewicza 11, 30-348 Kraków, Poland

Carola Hartel

Biophysics Department, GSI Helmholtzzentrum für Schwerionenforschung
Planckstrasse 1, 64291 Darmstadt, Germany

Ewa Gudowska-Nowak

Mark Kac Center for Complex Systems Research
Jagiellonian University, Kraków, Poland

Received 22 August 2023, accepted 17 October 2023, published online 27 October 2023

We dedicate this work to the memory of Professor Gerhard Kraft (1941–2023), a visionary physicist and a pioneer of heavy ion therapy developed at GSI.

Unlike biodosimetry of sparsely ionizing photons (X and γ rays), radiobiology and biodosimetry of densely ionizing (characterized by high linear energy transfer) heavy ions are still relatively poorly developed domains of science, despite a growing role of hadron beams in cancer therapy and an increasing frequency of exposure of humans to cosmic radiation. The most radiosensitive cell structure is the DNA which is responsible for storing genetic information. Interaction of radiation with the DNA leads to the formation of different types of DNA damage, the most severe of which are DNA double-strand breaks (DSBs). Damage to the DNA activates repair processes and their performance may be significantly reduced or stopped if the resulting damage is densely localized (clustered) on the distances of the order of nanometers. Erratic DNA repair leads to changes in the DNA structure causing rearrangements of the genome (chromosome aberrations), possibly resulting in subsequent cell death or induction of cancer. Relating models of chromosome geometry and their spatial position in the nucleus to a characteristic pattern of energy deposition in the biological target by incident radiation (track structure) allows us to predict the frequency and distribution of DSBs, displacement of formed fragments, and probability of translocation of genetic material between pairs of chromosomes. In this

work, we analyze results of the biophysical modeling of chromosome packing in the cell nucleus and confront them with cytogenetic experimental data evidenced by the former *in vitro* studies. In the quest for understanding effects of interphase chromosome geometry on the induction and frequency of chromosome aberrations, we have evaluated two models of the DNA polymer packing within the cell nucleus and validated the predicted exchange of genome with experimental findings.

DOI:10.5506/APhysPolB.54.10-A2

1. Introduction

1.1. Importance of statistical analysis for biodosimetry

Understanding of processes involved in the induction and transformation of radiation-induced biological damage is required for efficient design and improvement of methods of cancer treatment and radioprotection [1–4]. At the same time, heavy-ion radiobiology provides insights into evaluation of health risk related to human space exploration and possible exposure to charged energetic particles being constituents of galactic cosmic rays [4, 5].

The action of ionizing radiation in biological targets depends on radiation modality and results in alteration and breakage of chemical bonds, radiolysis of water, disruption of cell membrane integrity, and changes in active transport — all contributing to cell death and genetic mutations [6–8]. DNA double-strand breaks (DSBs) are considered to be the most severe radiation-induced damage for numerous biological endpoints, including cell inactivation or chromosomal aberrations. Not only the number of DSBs but also their spatial distribution appears to be crucial to understand the biological effects of radiation.

To investigate the impact of localized energy deposition on biological end-points, it is desirable to exploit models that allow for deduction of the influence of track structure on the formation of radiation damage in a given topology of a biological target (cell, cell nucleus, chromatin, DNA polymer). In cellular systems, it is difficult to separate the influence of track structure and its corresponding localized ionization events from the effects arising due to the three-dimensional organization of chromatin and its packing within the cell nucleus. At a micrometer scale, the energy deposition of X-rays and other photons is fairly uniform producing DNA damage in a stochastic manner. In contrast, the spatial distribution of the energy deposition after exposure to radiations with high linear energy transfer (LET), such as charged particles, is inhomogeneous [9–13] and reflects localized accumulation of deposit energy along the center of the particle path. Those differences in the radiation quality are further mirrored in the clustered DNA damages [6–8, 10, 14–17] following the particle radiations.

In the conventional X-ray radiobiology, the quantity parametrizing the ionizing radiation field is the absorbed dose, defined as the amount of energy delivered by radiation to matter per mass volume. Dose is treated as a collective, continuous parameter much larger in comparison to the quantum energy transferred in individual events of the Compton scattering, photo-effect, and pair production. Therefore, the biological response to photon radiation like X-ray, can be viewed as a reaction to a continuous perturbation function. For particle radiation, this is no longer valid even at macroscopically high doses. For heavy particles, the energy is transferred in local clusters: the DNA is hit by one particle track containing many electrons or it is not hit at all. The same occurs to cell nuclei: if an ion traverses a nucleus, many DNA lesions occur along the trajectory, or the cell nucleus is not affected by particles at all. Only incorporation of that "grainy" structure of particle irradiation, if applied to the analysis of experimental data, can lead to a correct description of the radiation response at all levels of DNA organization [14, 18–20]. Precise prediction and quantification of radiation-induced damage is of great importance for both radiation protection, particularly in open-space long-term manned missions, and for hadrontherapy of cancer with proton- and carbon-ion beams. Therefore, further improvements and possible refinement of existing models aimed at estimating the biological effectiveness of ions are indispensable.

The major objective of our prior investigations in this field was to use statistical physics methods and Monte Carlo simulations to foster biophysical modeling of radiation-induced damage at different scales of a biological target, and to compare theoretical results with experimental data to further calibrate the models. Accordingly, we have focused mainly on two topics:

— *Kinetics of processes leading to the formation of chromosomal aberrations, by taking into account the profile of damage distribution in irradiated cells that is characteristic of low and high LET radiation.*
Here, it was shown that the damage distribution reflects the track structure (ionization distribution) of the applied radiation type, something that could not be assumed *a priori*. The clustering of DNA double-strand breaks, and also of DNA fragment length, has been predicted by convoluting the deposited form of energy with the effect expected for similar local doses of photons [14].

— *Impact of chromosomal aberrations on synchrony of the cell cycle and the survival of damaged cells in subsequent mitotic cell divisions.*
It has been demonstrated that the delay of the mitotic cycle is correlated with the number of aberrations generated in a cell. The results obtained have been further used to estimate the relative biological effectiveness of ions [21].

As an example, Figs. 1 and 2 present results of our analysis [18, 19] demonstrating the inter-relationship between the track structure and the distribution of aberrations induced in human blood lymphocytes at different time-points after exposure. Figure 1, left panel, displays local dose distributions of 2 Gy photons (X-rays) to be compared with the right panel picturing dose distribution of 2.2 Gy of 177 MeV/u Fe-ions (3.7×10^6 ions/cm^2, LET = 355 keV/μm) at a micrometer scale, adequate to the size of the cell nucleus. For human lymphocytes the mean geometrical cross section of the cell

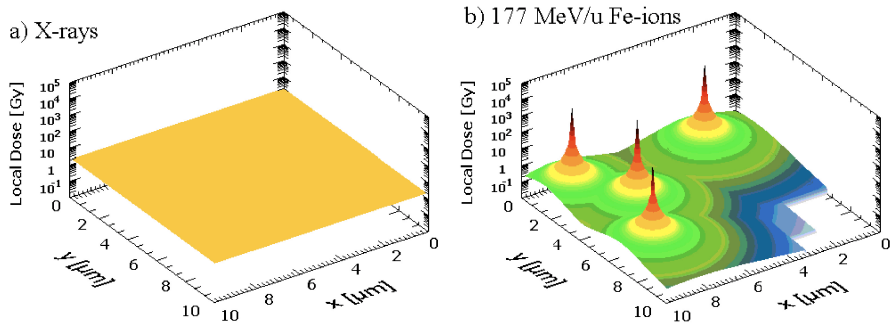

Fig. 1. Local dose distribution of photons and ions. The radial dose profiles have been evaluated by the use of the LEM model [13, 20] developed at GSI.

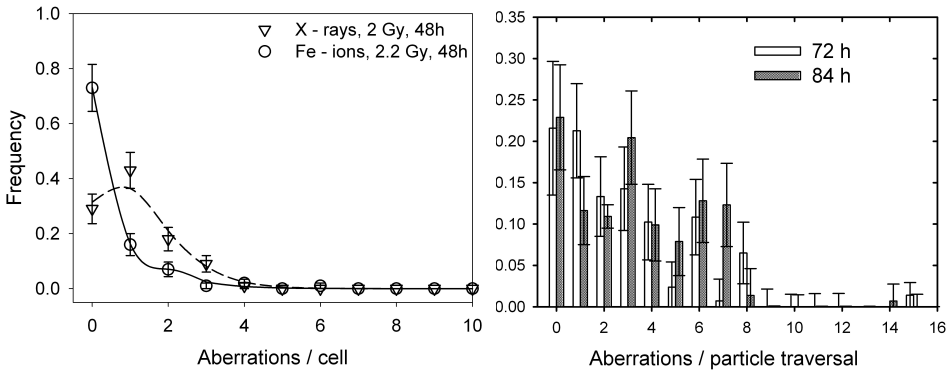

Fig. 2. Left panel: Distributions of chromosome aberrations induced by 2 Gy X-rays and 2.2 Gy of 177 MeV/u Fe-ions in 100 cells scored at 48 h after exposure (symbols) and the corresponding Poisson (X-rays) and Neyman-type-A (ions) fits to the experimental data. Error bars represent sample variations. Right panel: Distribution of aberrations produced by one particle hit $P(X_i = x)$ estimated from the Monte Carlo modeling of the time-dependent flow of aberrant cells through mitosis [15, 19] and fitted to experimental data at 72 h and 84 h after exposure. Errors are estimated by the method of propagation of uncertainty. For details of modeling, see Section 2.

nucleus is about 25 μm^2 and the nuclear region forms approximately 65% of the total cell area. Consequently, a particle fluence of 4×10^6 ions/cm^2 corresponds here to a mean number of one direct hit per lymphocyte cell nucleus. The radial local dose profiles of tracks [19, 20] clearly indicate nonuniform distribution of energy deposit after ion radiation. As a result, the observed distribution of biological damage, *i.e.* frequencies of chromosome aberrations in irradiated lymphocytes, as visualized by conventional staining techniques (*cf.* Fig. 3) follow the pattern of localized ionizations, as displayed in Fig. 2. Left panel of Fig. 2 shows exemplary distributions of chromosome aberrations induced by 2 Gy of X-rays and 2.2 Gy of 177 MeV/u Fe-ions in 100 cells scored at 48 h after exposure to radiation. In the right panel, frequencies of chromosome aberrations produced by one particle hit, as derived from the Monte Carlo (MC) distributions [19] of aberrations in 100 cells and fitted to experimental data at 72 h (84 h) are displayed. Progression of aberrations visible in mitotic cells has been obtained by the use of an MC model which incorporates delay of hit cells in mitosis as inferred from an experimental analysis of the mitotic index. Estimated frequencies of first metaphase cells carrying a distinct number of aberrations are plotted for various fixation times after irradiation. Non-hit cells are represented by a zero-frequency class which markedly differs for cells exposed to X-rays and ions. The difference reflects nonuniformity of the local dose distribution and simulated frequency spectra conform very well with experimental data [17, 18].

Statistical analysis of data coming from the above experiments has been further used to refine the Local Effect Model [13] exploited not only in estimation of DSBs yield induced by ion radiation but even more importantly, also in a treatment planning with carbon ions [4].

In terms of biophysical modeling, our interest has been focused on simulations of radiation damage in various hierarchical models of DNA organization. For example, in order to predict the number and distribution of aberrations at various times, we used the Monte Carlo technique tailored to include effects of delay in cell-cycle progression of injured cells [18]. First, by knowing the cross-sectional area of the biological target (*i.e.* assuming a spherical shape of the cell nucleus of a given diameter), we have estimated the average number of hits (traversals) per cell nucleus, at a given time t. For that purpose, the diameter value has been sampled from the Gaussian distribution around the mean. The whole population (say, 100 cells) has been then divided into subclasses with different numbers of hits, following the Poisson distribution with the intensity λ proportional to the local dose. In the next step, for each cell belonging to a specific class, its probability to reach mitosis at time t has been assigned by comparing the randomly generated frequency from the interval [0, 1] with the actual value obtained from the experimental data. According to the experimental observations,

hit cells are delayed in reaching mitosis, so that at earlier times, the fraction of cells with one or more hits will be smaller than at later times. The passage of an ensemble of 100 cells through mitosis has been further generated [15, 18, 19] by repeating the procedure at different times and by using the $\lambda(t)$ functional dependence, as determined from the experimental data sets.

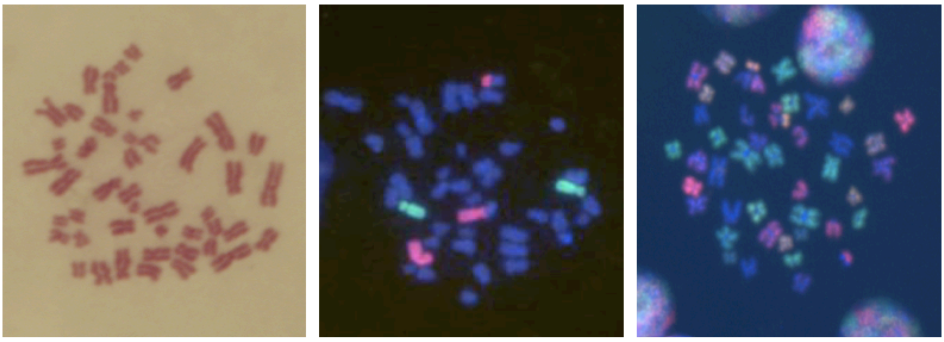

Fig. 3. Examples of different chromosome staining techniques (courtesy of S. Ritter): (a) Giemsa stained metaphase, (b) 2-color FISH stained metaphase, (c) mFISH stained metaphase (three-color display is shown). This method allows for full analysis of chromosomal interchanges. Proximity between any two chromosomes is estimated by the frequency with which they interact in radiation-induced interchanges. Significant deviations from the null hypothesis of random chromosome–chromosome spatial associations may be assessed by the use of dedicated Monte Carlo simulations [10]. More information about the distribution of DNA damage in individual chromosomes is of basic interest, as well as the exchange frequencies between chromosome pairs after irradiation. The former provides a better understanding of the induced damage and its repair in individual chromosomes (*e.g.* whether gene-rich chromosomes are more sensitive or resistant to radiation than gene-poor chromosomes). The latter provides information about the chromosome positioning in the interphase cell nucleus, as neighboring chromosomes are assumed to exchange more frequently than distant ones. The mFISH analysis can give information about both, the distribution of breakpoints among individual chromosomes and the exchange frequencies between chromosome pairs. Such data sets should be obtained and analyzed for different cell lines whose nuclei display distinctly different geometry (*e.g.* human fibroblasts and lymphocytes). Since acquisition of the information about exchanges visible in mFISH experiments is time and funds consuming, further development of physical models of chromosome positioning is indispensable to test the hypothesis about the formation and frequency of clusters of genome translocations among the groups of chromosomes [6, 8, 12], *cf.* Section 2.

1.2. Models of chromosome territories

The next step of biophysical modeling assumes using Monte Carlo and Molecular Dynamics methodologies in description of random interphase positioning of chromosomes within the cell nuclei. By convoluting spatial distribution of chromosomes with a track structure model and the statistics of damage event distributions, we aim to gain understanding of the frequency of translocations between pairs of chromosomes. If chromosomes are organized within the cell nucleus in territories which form clusters and if misrejoining of DSBs occurs mainly between neighboring chromosome territories (*i.e.* "open ends" do not travel long distances before reconnection to other ends [7]), the chromosomal clusters should be detectable on the basis of interchange data derived from the analysis of radiation-induced aberrations using mFISH or similar whole-genome staining methods [6].

Chromosome translocations caused by rearrangements of parts of genetic material between nonhomologous chromosomes are hallmarks of cancer cells and may indicate gene misregulation [6, 11, 22]. During interphase, chromosomes are confined to so-called territories [23]. In consequence, formation of translocations is fundamentally a spatial problem: rearrangement of genetic material between chromosomes requires physical interaction of partners. Accordingly, implications of the confined geometries and steric interactions on conformations of fully packed genome in spherical nuclei of lymphocytes have to be explored to understand the frequency of radiation-induced translocations. Since most likely, both topology and dynamics can lead to the efficient segregation of chromosomes [22, 24–26, 28–30], one of the major issues remains to model dynamics of interphase chromosomes subject to modified environmental conditions (*e.g.* medium polarity). The latter can be incorporated by *e.g.* varying parameters of the Lennard–Jones potential in molecular dynamics simulations of a chromatin-polymer model [27].

There is abundant experimental evidence indicating that arrangements of chromosomes in the eukaryotic cell nucleus is non-random and has been evolutionary conserved in specific cell types. Moreover, the radial position of a given chromosome territory (CT) within the cell nucleus has been shown to correlate with its size and gene density. Usually, it is assumed that chromosomal geometry and positioning result from the action of specific forces acting locally, such as hydrogen bonds, electrostatic, van der Waals, or hydrophobic interactions operating between nucleosomes and within their interiors. However, it is both desirable and instructive to learn to what extend organization of interphase chromosomes is affected by nonspecific entropic forces. In this study, we report on results of a coarse-grained analysis of a chromatin structure modeled by a simplistic approach.

Namely, we first adhere to purely statistical analysis of chromatin packing within a chromosome territory. On the basis of the polymer theory, the chromatin fiber of a diameter of 30 nm is approximated by a chain of spheres, each corresponding to about 30 kbp (*cf.* Fig. 4). Random positioning of the center of the domain is repeated for 1000 spherical nuclei. Configuration of the domain is determined by a random packing of a polymer (a string of identical beads) in estimated fraction of space occupied by a chromosome of a given length and mass. The degree of condensation of the chromatin fiber is modeled by changing the length of the string: *e.g.* loosening of the structure is achieved by distributing the chromosome mass into a higher number of smaller beads and tighter configuration corresponds to a lower number of fragments (balls) with a bigger radius. Additionally, for each configuration, a degree of possible overlapping between domains is assumed. This procedure effectively intensifies loosening/tightening of the chromosome structure by changing the radial dimension of the domain while keeping a constant volume of the polymer chain. Such a positioning model is further confronted with a minimalistic molecular dynamics model on a similar structure, in which a chain of beads becomes connected by entropic spring energy and subjected to thermal fluctuations. Comparison of both Monte Carlo (MC) and Molecular Dynamics (MD) models allows us to discuss the variability of possible configurations as observed in static and dynamic models of chromosome territories along with the effect of compaction and relative arrangements of territorial polymer structures.

Fig. 4. An oversimplified, coarse-grained, and knot-free model of chromatin structure as used in the MC studies of chromosome positioning within the cell nucleus. The details of the polymer structure are not taken into account beyond the typical length $L_{\mathrm{p}} = 300$ nm representing an average diameter of the "swollen" chromatin fibre in G0/G1 phase. The mass of a genome is distributed uniformly according to the length of a chromosome. According to the model, each chromosome of the diploid human genome is approximated by a chain of spherical beads, each of radius $R = 0.15$ μm.

The volume of a given chromosome configuration can be understood according to the Edwards hypothesis [32] which links configuration with the distribution of "grains", *i.e.* of tiny beads constituing interphase chromatin polymer. The distribution of grains over the available volume states (subject

to external constraints such as stability under gravity and that the grains are impenetrable) gives rise to a volume of configuration. In a formal analogy to energy, the volume V may be used to define the thermodynamic state of the system and the derivative of entropy with respect to V introduces the inverse "compactivity", the parameter isomorphic to the inverse temperature in a canonical formulation of the Boltzmann equilibrium ensemble [31]. Such a compactivity parameter may serve as a measure of packing and can discriminate among different classes of confinement, as has been discussed elsewhere [29, 30].

Here, we refer solely to the analysis of statistical (MC) and dynamic (MD) models and confront simulated data of chromosome positioning within the spherical nucleus of human lymphocytes with experimental results.

Our ultimate goal is to shed light on the effect of chromosome packing within the cell nucleus on the frequency of aberrations induced after irradiation with ions and photons (X-rays). Accordingly, the final stage of modeling refers to an overlap of track structure with a biological target of interest.

The paper is organized as follows: After briefing advancements in stochastic modeling in biodosimetry and recent investigations on arrangements of chromosome territories in interphase (Section 1), we proceed with presenting statistical approach and numerical schemes used to analyze and model experimental data (Section 2). Most important findings of the devised analysis are introduced in Section 3 and followed by conclusions in Section 4.

2. Materials and methods

2.1. Modeling induction of chromosome aberrations

For the analysis of the distribution of cytogenetic damage among irradiated cells, the compound Poisson statistics has been used which combines the concept of primary radiation acts (hits in biological target) with secondary events, representing induction of cellular damage. Accordingly, in this approach, the (flux) of aberrant cells (or chromosome aberrations) through mitosis can be modeled as a renewal process [15, 18, 19]. The number of events (*e.g.* number of aberrant cells, number of aberrations) at a given time t is then represented as a random sum of independent and identically distributed random variables, $x(t) = \sum_{j=1}^{n(t)} X_j$ with $n(t) = \min\left\{n : \sum_{j=1}^{N} T_j > t\right\}$ reflecting the number of traversals through a cell nucleus and sampled from a nonhomogeneous (time-dependent) Poisson process. As estimated at time t, each act leads to a statistically-independent formation of X_j secondary events (*e.g.* aberrations). With an increasing number of particle hits per cell nucleus, more chromosome damage is produced. In effect, heavily damaged cells are delayed and enter mitosis later than slightly damaged or undamaged

cells [15, 21]. The resulting probability distribution of x follows then a general law for which the moment generating function $\Phi_{x(s)}$ satisfies the relation $\Phi_{x(t)}(u) \equiv \left\langle \mathrm{e}^{ux(t)} \right\rangle = \Phi_{n(t)}\left[\Phi_X(u)\right]$, where brackets denote the distribution average. By assuming $\langle n(t)\rangle = \lambda(t)$, $\langle X_i\rangle = \mu$ with an average number of aberrations visible at time t, $\langle x(t)\rangle = \lambda(t)\mu$, the logarithm of $\Phi_{x(t)}(u) \equiv \left\langle \mathrm{e}^{ux(t)} \right\rangle$ can be rewritten as $\ln \Phi_{x(t)}(u) = \left[\frac{\langle x(t)\rangle}{\langle X_i\rangle}\left\{\exp\left(\langle X_i\rangle[\mathrm{e}^{-u} - 1] - 1\right)\right\}\right]$. This allows to derive factorial moments of the distribution $p(x,t) = p(x(t))$ by subsequent differentiation of $\Phi_{x(s)}(u)$ and substitution $u = 0$. The corresponding fits to the experimental data at a given time point t can be performed by the use of a recurrence formula [19] derived from the moment-generating function. Location of damage in events (ionizations) is achieved by the use of the track structure models [13, 18]. Yield of specific events, like *e.g.* DNA double-strand breaks, or induction of aberrations due to direct effects can be further obtained from a superposition of a track structure (or its local dose-deposition equivalent) with a specific target model (DNA at a given level of its spatial organization).

2.2. Modeling organization of interphase chromosomes

2.2.1. Monte Carlo code for chromosome positioning in cell nucleus

At this level of modeling, the detailed structure of chromatin fiber is not taken into account. Instead, each simulated chromosome in the G0/G1 phase is positioned in a spherical domain, the volume of which is estimated based on spatial restraints to be satisfied [23, 24]: The cellular nucleus is represented as a sphere of radius 2.8 μm filled with randomly distributed spherical domains containing chromosomes. Chromosome sections in the extended forms have been assumed to form cylinder-like objects of the diameter 300 nm, see Fig. 4. The length of a chromosome has been chosen according to its mass content and the inner structure has been mapped into a series of beads, each of a constant radius $R = 0.15$ μm. Random positioning of the model 23 pairs of chromosomes in a cell nucleus has been further analyzed in terms of the radial distance between the nucleus center and the center of the domain, *cf.* Figs. 5 and 6.

2.2.2. Polymer chromosome model and Molecular Dynamics simulations

Self-avoiding, semiflexible chromatin segments and chromosomes have been also modeled in the simplest possible polymer-alike scenario [28, 30, 32, 34], as chains of beads, each bead (monomer) of mass m and radius $R = 150$ nm. The total length of a model chromosome conforms with the known mass of a given chromosome consisting of n beads. Integrity of a chromosome has been assured by assuming harmonic interactions between

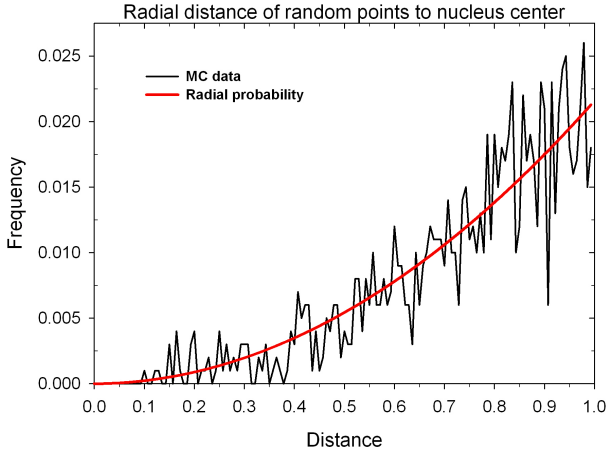

Fig. 5. Exemplary uniformly random radial distribution of 1000 points in a sphere of radius 2.8 μm. Solid line represents a corresponding theoretical (normalized) distribution of radial distances in a sphere.

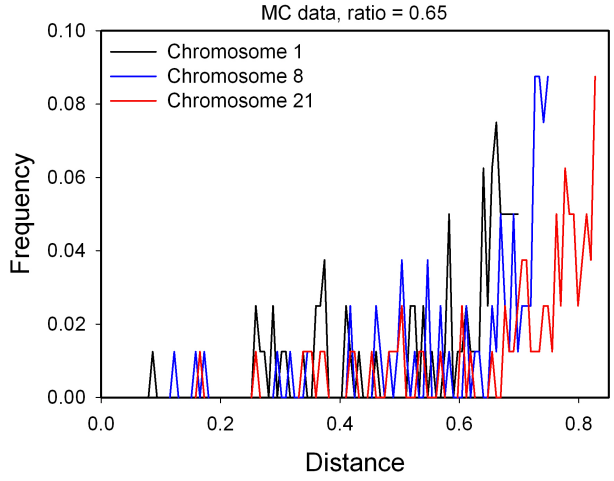

Fig. 6. Sample random positioning of chromosomes 1, 8, and 21 in a spherical lymphocyte. Total DNA content has been assumed to fill 65% of nuclear volume. Results for simulated 100 nuclei.

the nearest neighbors along the chain

$$F_{H0} = -2H_0 \left(\frac{r}{2R} - 1 \right) , \tag{1}$$

where r denotes distance between centers of neighboring parts and H_0 is a proportionality parameter. To avoid beads interpenetration, the additional

repulsive force starts acting when $r < 2R$

$$F_{EV0} = \begin{cases} -E_0 \frac{r}{R^2} \left[\left(\frac{r}{2R} \right)^2 - 1 \right], & \text{if } r < 2R, \\ 0, & \text{otherwise}. \end{cases} \tag{2}$$

Interaction (1) is assumed to occur only between the nearest neighbors along the chain, whereas (2) includes potentially all components of a chromosome. Conservation of a (model) spherical shape of the whole chromosome is assured by another harmonic force, which is switching on only for outlying monomers. The form of this interaction is similar to (1) but uses parameter R_{Ch} equal to a chromosome radius varying between 530 nm and 910 nm

$$F_{H1} = \begin{cases} -2H_1 \left(\frac{r}{R_{\mathrm{Ch}} - R} - 1 \right), & \text{if } r > (R_{\mathrm{Ch}} - R), \\ 0, & \text{otherwise}. \end{cases} \tag{3}$$

Here, r is a distance between a sphere center and a chromosome mass center. The force is switching on for only those outlying monomers that recede too much from the chromosome mass center. Additional dynamics takes place at the level of a nucleus containing 46 chromosomes. The nucleus radius was chosen to be $R_N = 2800$ nm. Its spherical shape is constrained by another harmonic interaction not allowing a chromosome to move too far away

$$F_{H2} = \begin{cases} -2H_2 \left(\frac{r}{R_N - R_{\mathrm{Ch}}} - 1 \right), & \text{if } r > (R_N - R_{\mathrm{Ch}}), \\ 0, & \text{otherwise}. \end{cases} \tag{4}$$

As previously, the force is applied only to chromosomes crossing the nucleus border.

Time evolution of chromosomes is further derived using Molecular Dynamic techniques, specifically the velocity Verlet algorithm. The singular simulation step consists of two phases. The first one concerns the internal dynamics of chromosomes. Here, to assure thermal equilibrium, additional noise and dissipation terms have to be added

$$\vec{F} = \vec{F}_{\mathrm{D}} - m\gamma\vec{v} + \vec{\xi}, \tag{5}$$

where F_{D} is deterministic force (sum of all mechanical forces acting within the chromosome structure, as described above), m is a mass of a single chromosome component (ball), v is its velocity, and γ is a friction constant. $\vec{\xi}$ is a vector of Gaussian random numbers $\{\xi_1, \xi_2, \xi_3\}$ with vanishing average and variance fulfilling fluctuation–dissipation theorem

$$\mathrm{var}(\xi_i) = \frac{2m\gamma k_{\mathrm{B}} T}{\Delta t}, \qquad \text{for } i = 1, 2, 3, \tag{6}$$

where T is absolute temperature, k_{B} is a Boltzmann constant, and Δt denotes the time step used to integrate equations of motion. The second phase of the algorithm step plays a role at the level of chromosomes. First, basing on positions and velocities of the monomers, we calculate those values for each chromosome. Then, forces (3) and (4) are applied, and all kinetics are translated back to the monomers level.

For the purpose of simulations, dimensionless units have been used. Since we do not have any information about the relative strength of interactions described above, we assume that all the components are comparable. Therefore, $H_0 = H_1 = H_2 = E_0 = k_{\mathrm{B}}T$, where $k_{\mathrm{B}}T$ is an energy unit. The time and frequency units correspond to periodic oscillations of beads caused by interaction (1). Thus, $\omega_0 = \frac{\sqrt{2H_0}}{2R}$ and $t_0 = \frac{2\pi}{\omega_0}$. The friction constant was equal to $\gamma = 10\,\omega_0$, which corresponds to slightly overdamped dynamics. The time step has been chosen as $\Delta t = 0.001\,t_0$ and the mass unit has been m. Typically, simulations have been carried out for $10^6 t_0$ time steps to ensure that the simulated nucleus reaches its thermal equilibrium state. This simple dynamic model of a chromosome structure has been tested against the static MC model to detect possible differences (*cf.* Fig. 7) in chromosome positioning caused by excluded volume effects and physical interactions.

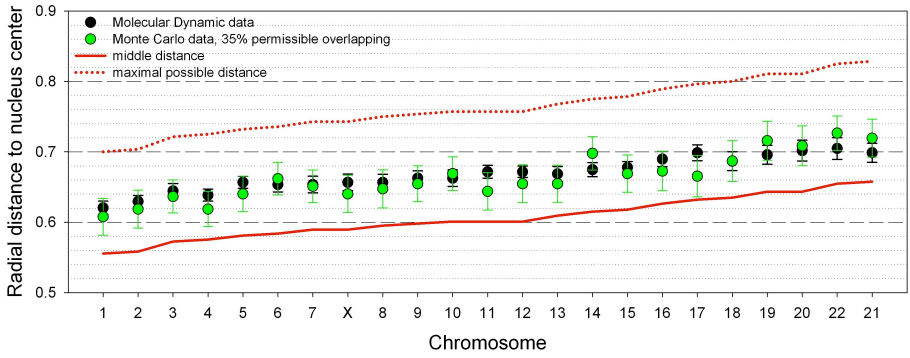

Fig. 7. Radial distances to the nucleus center obtained from a sample configuration of chromosome packing in an idealized spherical nucleus of human lymphocytes, and derived from independent MC and MD studies. DNA content has been fixed to fill 65% of the nuclear volume and 100% of the volume of domains. For simulations of chromosome territories, a spherical domain model has been assumed (see the text).

2.2.3. Spatial distribution of DSBs from the Local Effect Model (LEM)

Frequency of gene translocations between pairs of chromosomes and induction of chromosome aberrations is determined from the initial DSB distribution pattern, which in turn, depends on combination of particle traversals

and ionization events pertinent to the track structure. In order to generate a spatial distribution of DSBs in a model cell nucleus after irradiation with 2 Gy X-rays and corresponding dose (2.2 Gy) of ions, an extended version of the LEM model has been used, as implemented by the GSI group [13, 33]. The center of the simulated track has been assumed to traverse through the nucleus center, although its azimuthal direction has been chosen uniformly random with an angle $\alpha \in [0, 360°)$. To further discriminate between effects induced by a random packing of chromosomes in nuclear volume and variations of the track, we have performed statistical analysis of

— geometries of 100 simulated target models (cell nuclei) convoluted with 100 independently simulated tracks, each inducing on average the same amount of DSBs (*Model 1*),

— 100 model targets overlayed with the same one-track structure (*Model 2*),

— identical 100 targets (the same topology of chromosome organization and positioning in a cell nucleus) convoluted with 100 different tracks (*Model 3*).

At all stages of simulations, the model of DSBs induction has been calibrated by referring to experimental data [6, 15, 18, 19]. In particular, in line with the analysis of production and distribution of aberrations in resting and cycling human lymphocytes following Fe-ion irradiation [15], primary radiation damage has been quantified as the number of chromatin fragments in excess of that measured in non-irradiated control cells. This resulting number of excess PCC fragments/cell has been further adopted as an indicator of the number of DBSs induced by irradiation. Data obtained for the G0-lymphocytes showed [6, 15, 18, 19] that for all exposure conditions, the number of fragments/cell increased linearly with fluence or dose. Comparison of the initial chromatin breakage produced by a mean number of one particle traversal per cell nucleus revealed that one Fe-ion traversal resulted in about 28 excess fragments/cell/hit which in the course of time and possible repair, relaxed to about 15 excess fragments/cell/hit 24 h after exposure [15]. In contrast, a similar dose of X-rays (2 Gy) resulted in about 18 initial excess fragments/cell and dropped to about 4.8 excess fragments per cell after 24 h. Accordingly, the indicative DSB rate induction of about 28 DSBs per one particle hit has been used in the implemented LEM procedure aimed to characterize statistics of spatial distribution of breaks in cellular and nuclear domains. In brief, intersection of simulated track structures with a disc-like, cylindrical geometry (an average diameter 10 μm) of a lymphocyte allows to predict a spatial distribution of damage within the cell volume [13]. In the next step, localization and statistics of breaks within the cell nucleus

can be analyzed by overlapping the pattern of breaks with a spherical volume of a cell nucleus ($r = 2.8$ μm). In consequence, this analysis estimated an average of 15 breaks located directly in the volume of the cell nucleus.

3. Results

3.1. Polymer modeling of chromosome organization

Chromosome territories formed by different chromosomes are commonly believed to have non-random arrangement influenced by gene density and the chromosome mass. In effect, arrangements of chromosomes within the volume of a spherical nucleus, and in particular their spatial entanglement, are expected to influence interactions between radiation-induced breaks and to correlate with relative participation of various chromosomes in interchanges [10, 11, 34].

For the purpose of quantifying the effect of chromatin compaction and curling on the positioning of chromosomes in distinct territories, we have elaborated a probabilistic scheme of folding based on a minimal polymer model of decondensed chromosomes. The latter takes into account the self-avoidance and bending stiffness of the fibre together with the linear connectivity of polymer units (*cf.* Section 2.2.2). Figures 7 and 8 summarize our findings based on the MC/MD modeling: Normalized distances of the domain centers from the center of a nucleus are comparable for both modes of modeling and result in similar trends in positioning of chromosomes. Since the MD simulations of Brownian dynamics are much more time consuming than the MC analogs, for the purpose of further investigations, we have limited our analysis to the superposition of LEM-derived distribution of breaks over the MC-generated nuclear structure (see Section 2.2.1).

3.2. Correlation of spatial distribution of DSBs with arrangements of chromosomes in the nucleus territory

For a given pattern of Fe-ion traversal, the local dose deposition can be derived from the radial profile of the track. Frequencies and distribution of the total number of DSBs following that pattern have been calculated using the amorphous track structure LEM model [33]. In turn, to model distributions of DSBs observed after irradiation with photons, we have assumed a homogeneous scattering of the same number of breaks among 100 nuclei. This step of modeling requires partitioning of 100 targets into fractions with 0, 1, 2, and more hits, following the Poisson distribution with an average one particle traversal per cell nucleus. Outcomes of simulations based on these assumptions reflect the pattern of DNA damage observed after X-ray irradiation with a uniform spatial distribution of deposited energy.

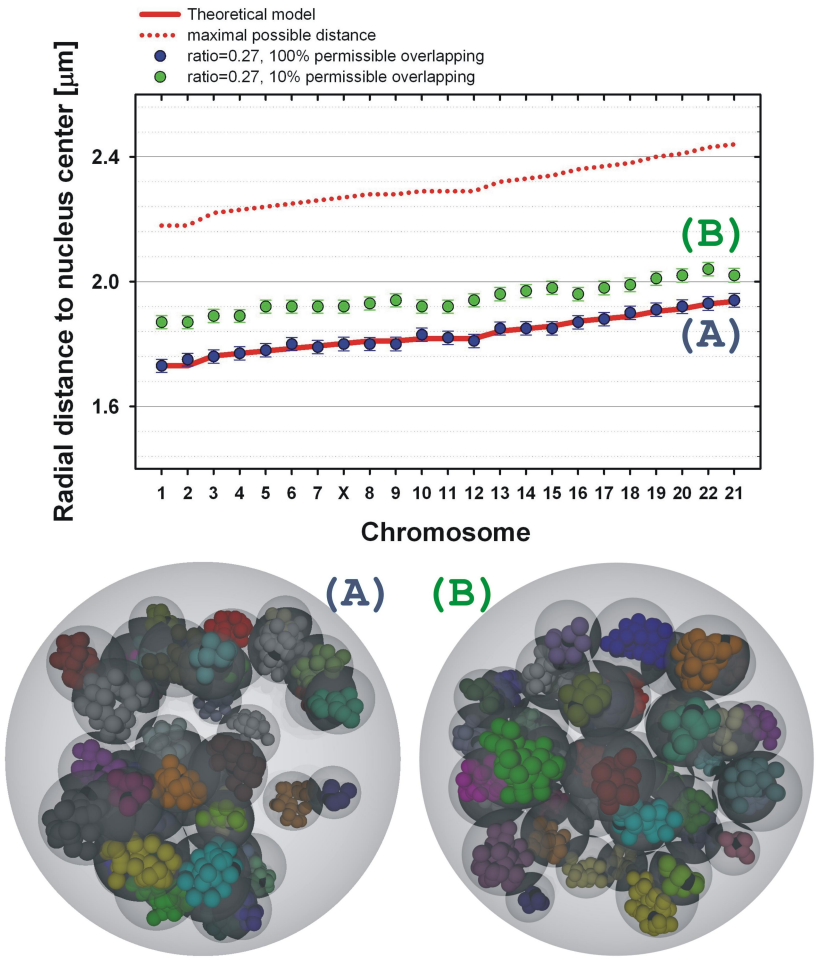

Fig. 8. Sample configuration of chromosome packing in an idealized spherical nucleus of human lymphocytes. For simulations of chromosome territories, a spherical domain model has been assumed. In a randomly chosen domain, a subcompartment model of an interphase chromosome is presented.

Results for 100 simulated nuclei of various organization, each traversed by a projectile in a different geometry with respect to the target (*Model 1*) are summarized in figure 9. Distribution of DSBs in 100 cells is roughly Poisson with the mean of about 15 DSBs/cell, in accord with experimental observations [15]. The effect of radial positioning of chromosomes with respect to the nucleus center has been further analyzed by overlapping the same track structure with 100 different nuclear arrangements (*Model 2*). Participation of various chromosomes in formation of aberrations in dam-

aged cells remains in this case similar to the pattern observed in *Model 1*, see figures 10 and 11, and strongly deviates from the predictions based on the simulated homogeneous distribution of breaks.

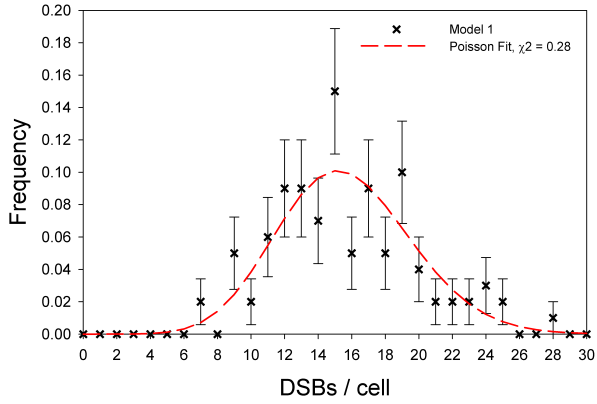

Fig. 9. Distribution of the total number of DSBs in 100 cells (mean = 15.68) obtained from numerical simulations following *Model 1*. Standard deviation of the sample is 4.23.

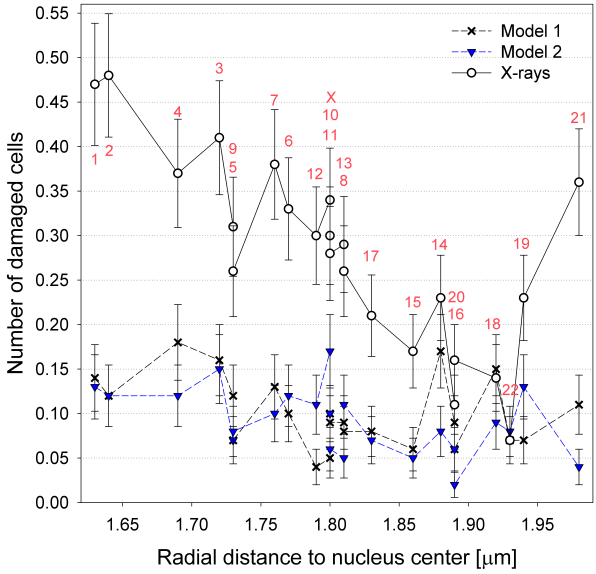

Fig. 10. Number of damaged cells in which breaks within a given chromosome have been registered. Data points represent results of simulations for *Models 1* and *2* expressed as percentage of damaged cells. Open symbols display data simulated for uniform space distribution of 15 breaks/cell nucleus, typical for exposure to X-rays. Red numbers in the top graph label the participation of various chromosomes.

An interesting comparison is indicated in distribution of breaks per chromosome per cell resulting from models of localized (in the case of ions) *versus* uniform (for photons) depositions of ionizing events. Figures 11 and 12 show that local proximity of ionizations after irradiation with ions results, on one hand side — in a higher frequency of intact (non-hit) cells with respect to the zero class predicted by uniform (Poisson) distribution, and on the other — in much broader, dispersed distribution of breaks in a population of 100 simulated cells.

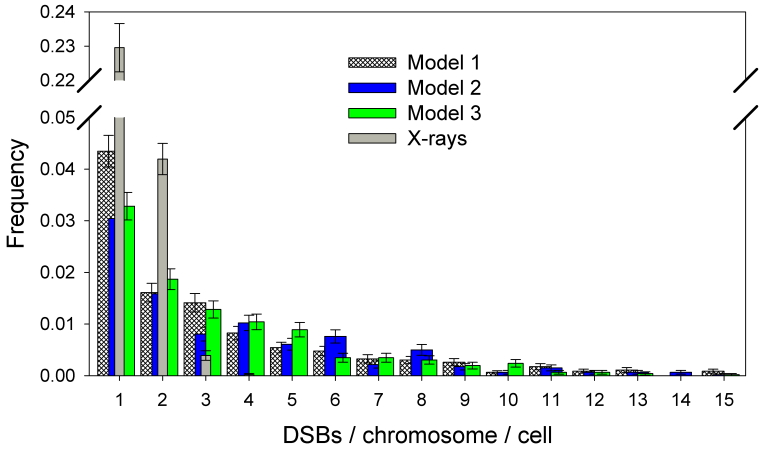

Fig. 11. Distribution of 15 breaks in modeled nucleus-track arrangements (see the text). For comparison with X-rays, we have assumed 15 breaks distributed uniformly within the nuclear volume.

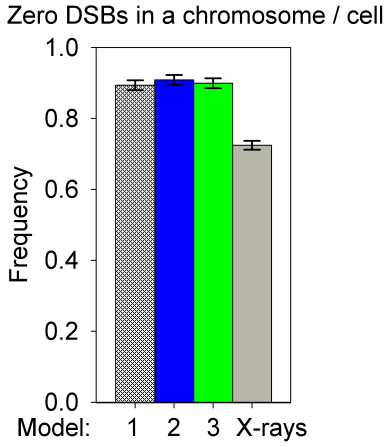

Fig. 12. Frequency of non-hit (undamaged) cells derived from the simulations. For details, see the text.

Misrejoining patterns leading to aberrations have been further modeled by a mechanistic approach described by Sachs *et al.* [34, 35]. In brief, distribution of DSBs on chromosome structures produces free ends which can be correctly or incorrectly rejoined, when the DSB rejoins with its original partner or misrejoins with another DSB. In the simplest form of the breakage-and-reunion model [35], all free ends undergo restitution or participate in illegitimate reunions. Out of the chromosome-free-ends formed, only those located within a certain distance may be rejoined by either restoring the original structure or producing an aberration. A rearranged chromosome produced in a complete (no free ends left) reunion and exchange process either possesses a telomere at each end or forms a closed ring. The set of all rearranged chromosomes produces the final configuration of aberrant and restituted entities. Contemporary experimental assays based on multiplex fluorescent *in situ* hybridization (mFISH) allow for painting of chromosomes thus elucidating fragments coming from misrejoins and complementing karyotype changes detected by the standard Giemsa technique (*cf.* Section 1.1).

The final stage of our modeling aimed to confront simulated patterns of aberrations, as experimentally detected by either the Giemsa or mFISH techniques. The first step of this analysis yields the probability of rejoining. Its assignment to any pair of induced free ends is based on estimated (and normalized to one) distribution of distances between the breaks. Accordingly, the faithful or illegitimate rejoinings become influenced by the

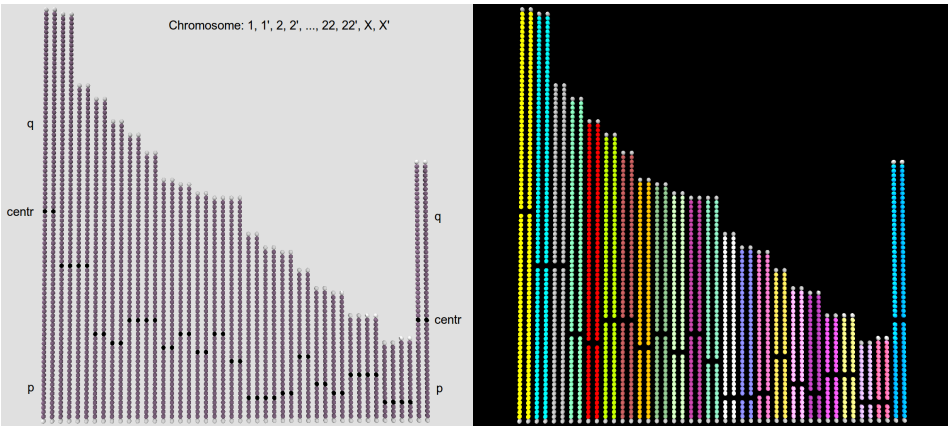

Fig. 13. Models of chromosomes analyzed in the paper. Symbols p and q denote a short and a long chromosome arm, respectively. Grey spheres represent telomers (chromosome terminus) and black ones indicate the centromers' positions. Left figure shows an exemplary slide of aberration-free chromosomes, as observed in a standard Giemsa staining. Right figure refers to the same set in a model FISH staining where every pair of chromosomes is painted with a different color.

proximity of free ends. As a result, the employment of this procedure allows us to determine the idealized pattern of aberrations, as exemplified in Fig. 14 in comparison with the control, Fig. 13.

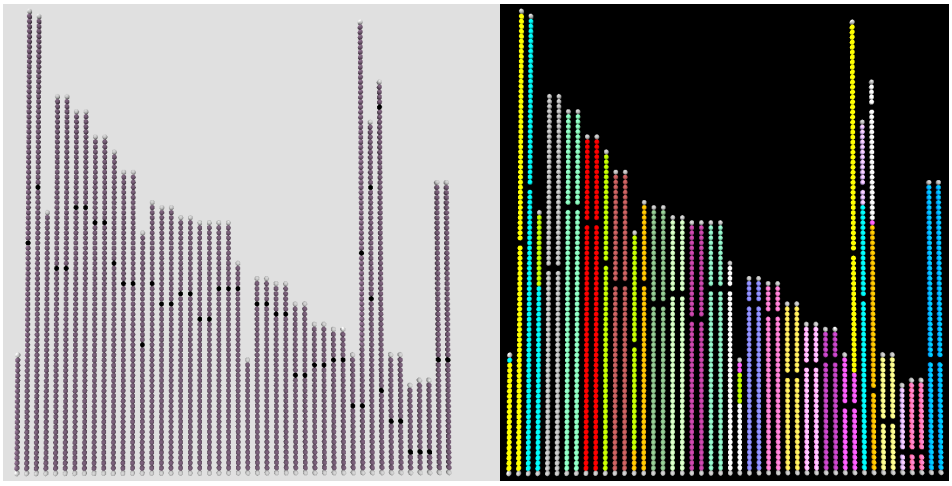

Fig. 14. Results of modeling radiation-induced translocations (exchanges) among the group of chromosomes (*cf.* Fig. 13). Right figure shows a model rearrangement of broken arms among the group of chromosomes hit by 1 particle traversal. Resulting misrejoinings, as observed in the FISH staining, involve various colors indicating participation of various chromosomes. Non-homologous end joining has been modeled based on the spatial juxtaposition of genomic loci as derived from the spatial distribution of radiation-induced breaks, see the text.

4. Discussion

Chromosome aberrations are large-scale illegitimate rearrangements of the genome and ionizing radiation is a potent inducer of those exchanges. In various former studies, it has been indicated that formation of chromosome territories in cell nuclei and their mutual proximity have an impact on the frequency of radiation-induced aberrations. Understanding the chromosomal damage induced by sparsely as well as densely ionizing radiation is an important research topic, as environmental, medical, and occupational radiation-exposure can be a potential health risk. It is known that the biological effects of sparsely and densely ionizing radiation can be quite different, as equal physical doses have different biological effects (described by the relative biological effectiveness — RBE) and they induce different chromosome aberration patterns with densely ionizing radiation inducing a higher fraction of complex aberrations (*cf.* [40, 41]). Chromosomal aberration analysis is a time-consuming and (in the case of mFISH) expensive method, thus

modeling is a valuable complement to experimental data to better understand the biological consequences of densely and sparsely ionizing radiation exposure.

Our work was meant to present contemporary approaches to biophysical modeling which simulates the induction of chromosome aberrations by different radiation modalities, such as particles and photons. Special emphasis has been devoted to pointing out distinctive differences between the distribution of biological damage caused by low- and high-LET exposure. An approximate stochastic MD description of a Rouse-like polymer model confined in a spheric domain allowed us to follow the frequency of encounter events when chains representing different chromosomes intertwined within the cell nucleus being simultaneously traversed by projectiles' tracks. The spatial distribution of the latter and corresponding induction of breaks following a local dose distribution have been simulated based on the LEM model developed at GSI, one of a few models developed to predict the response to charged particle radiation for all clinically-relevant situations [36, 37]. Different exposure setups are often used to study the relation between biological responses and LET [38, 39]. Our statistical tests are grounded on three models adapted for analysis of effects of random packing of chromosomes in nuclear volume and variations of the track captured degree of uncertainties in derived frequencies of induced breaks. It has been shown that chromatin compaction influences DNA repair. Further developments of the model could take this into account by distinguishing between euchromatin and heterochromatin, as it is done in the case of other models of radiation-induced DNA damage [42]. In particular, it has been argued that in decondensed eurchromatin, a lower proportion of direct strand breaks is observed in line with fewer DNA targets per unit volume crossed by a given projectile. Therefore, differences in induced DSB yield should be observed, determined by the degree of chromatin compaction and concentration of histone proteins which play a role of radical scavengers. These problems could be addressed in future simulations aimed to provide better models of chromatin structure.

Physical differences in DNA damage represent only the first stage in radiation's biological effects which are further processed dependent on the cell's ability to detect, respond, and repair the damage. Mechanistic and stochastic models, as described here, can provide a basis for more advanced approaches to probabilistically link early DNA damage with biological effects including the type of damage complexity, misrepair kinetics, and cell survival.

In conclusion, computer simulations offer new insights into experimentally-observed and clinically-relevant endpoints enabling at the same time a better understanding of processes involved in the biological response to ionizing radiation.

The Authors acknowledge the long-lasting collaboration and many fruitful discussions with Drs. Sylvia Ritter, M. Scholz, and T. Friedrich from the Biophysics Department, GSI. The research for the publication is supported in part by the Strategic Programme Excellence Initiative at the Jagiellonian University in Kraków, Poland.

REFERENCES

[1] G. Kraft, S.D. Kraft, «Research needed for improving heavy-ion therapy», *New J. Phys.* **11**, 025001 (2009).

[2] M.H. Holzscheiter *et al.*, «A community call for a dedicated radiobiological research facility to support particle beam cancer therapy», *Radiother. Oncol.* **105**, 1 (2012).

[3] M.A. Tabocchini, A. Campa, V. Dini, «DNA and Cellular Effects of Charged Particles», *Health Phys.* **103**, 547 (2012).

[4] E. Fokas, G. Kraft, H. An, R. Engenhart-Cabillic, «Ion beam radiobiology and cancer: Time to update ourselves», *Biochim. Biophys. Acta* **1796**, 216 (2009).

[5] M. Durante, F. Cucinotta, «Heavy ion carcinogenesis and human space exploration», *Nat. Rev. Cancer* **8**, 465 (2008).

[6] S. Ritter, M. Durante, «Heavy-ion induced chromosomal aberrations: A review», *Mutat. Res.* **701**, 38 (2010).

[7] B. Jakob, J. Splinter, M. Durante, G. Taucher-Scholz, «Live cell microscopy analysis of radiation-induced DNA double-strand break motion», *Proc. Natl. Acad. Sci.* **106**, 3172 (2009).

[8] M.S. Sasaki, «Advances in the biophysical and molecular bases of radiation cytogenetics», *Int. J. Radiat. Biol.* **85**, 26 (2009).

[9] H. Nikjoo, S. Uehara, D. Emfietzoglou, A. Brahme, «Heavy charged particles in radiation biology and biophysics», *New J. Phys.* **10**, 075006 (2008).

[10] J. Arsuaga *et al.*, «Chromosome spatial clustering inferred from radiogenic aberrations», *Int. J. Radiat. Biol.* **80**, 507 (2004).

[11] W. Friedland, P. Jacob, P. Kundrat, «Stochastic simulation of DNA double-strand break repair by non-homologous end joining based on track structure calculations», *Radiat. Res.* **173**, 677 (2010).

[12] C.K. Wang, «The progress of radiobiological models in modern radiotherapy with emphasis on the uncertainty issue», *Mutat. Res.* **704**, 175 (2010).

[13] T. Friedrich *et al.*, «Calculation of the biological effects of ion beams based on the microscopic spatial damage distribution pattern», *Int. J. Radiat. Biol.* **88**, 103 (2012).

[14] T. Elsässer *et al.*, «Biophysical Modeling of Fragment Length Distributions of DNA Plasmids after X and Heavy-Ion Irradiation Analyzed by Atomic Force Microscopy», *Radiat. Res.* **169**, 649 (2008).

[15] J. Deperas-Standylo *et al.*, «Production and distribution of aberrations in resting or cycling human lymphocytes following Fe-ion or Cr-ion irradiation: Emphasis on single track effects», *Adv. Space Res.* **50**, 584 (2012).

[16] E. Nasonova, E. Gudowska-Nowak, S. Ritter, G. Kraft, «Analysis of Ar-ion and X-ray-induced chromatin breakage and repair in V79 plateau-phase cells by the premature chromosome condensation technique», *Int. J. Radiat. Biol.* **77**, 59 (2001).

[17] E. Gudowska-Nowak, E. Nasonova, S. Ritter, M. Scholz, «Chromosome fragmentation after irradiation with C ions», *Radiother. Oncol. Suppl. 2* **73**, S123 (2004).

[18] J. Deperas-Standylo *et al.*, «Time-course of aberrations and their distribution: impact of LET and track structure», *Eur. Phys. J. D* **60**, 93 (2010).

[19] J. Deperas-Standylo, E. Gudowska-Nowak, S. Ritter, «Stochastic modelling for biodosimetry: Predicting the chromosomal response to radiation at different time points after exposure», *Eur. Phys. J. D* **68**, 204 (2014).

[20] M. Scholz, G. Kraft, «Calculation of Heavy Ion Inactivation Probabilities Based on Track Structure, X Ray Sensitivity and Target Size», *Radiat. Protect. Dosim.* **52**, 29 (1994).

[21] A. Ochab-Marcinek, E. Gudowska-Nowak, E. Nasonova, S. Ritter, «Modeling radiation-induced cell cycle delays», *Radiat. Environ. Biophys.* **48**, 361 (2009).

[22] K.J. Meaburn, T. Misteli, «Chromosome territories», *Nature* **445**, 379 (2007).

[23] Y. Markaki *et al.*, «Functional nuclear organization of transcription and DNA replication: a topographical marriage between chromatin domains and the interchromatin compartment», *Cold Spring Harb. Symp. Quant. Biol.* **75**, 475 (2010).

[24] D. Marenduzzo, C. Micheletti, E. Orlandini, «Biopolymer organization upon confinement», *J. Phys.: Condens. Matter* **22**, 283102 (2010).

[25] J. Dorie, A. Stasiak, «Topological origins of chromosomal territories», *Nucleic Acids Res.* **37**, 6316 (2009).

[26] H. Jerabek, D.W. Heermann, «Expression-Dependent Folding of Interphase Chromatin», *PLoS One* **7**, e37525 (2012).

[27] A. Rosa, R. Everaers, «Structure and dynamics of interphase chromosomes», *PLoS Comp. Biol.* **4**, e1000153 (2008).

[28] M. Tark-Dame, R. van Driel, D. Heermann, «Chromatin folding — from biology to polymer models and back», *J. Cell Sci.* **124**, 839 (2011).

[29] M. Barbieri *et al.*, «Polymer models of chromatin organization», *Front. Genet.* **4**, 113 (2013).

[30] J. Langowski, «Polymer chain models of DNA and chromatin», *Eur. Phys. J. E* **19**, 241 (2006).

[31] Ch. Song, P. Wang, H.A. Makse, «A phase diagram for jammed matter», *Nature* **453**, 629 (2008).

[32] S.F. Edwards, C.C. Mounfield, «The statistical mechanics of granular systems composed of spheres and elongated grains», *Physica A* **210**, 290 (1994).

[33] T. Friedrich *et al.*, «Calculation of the biological effects of ion beams based on the microscopic spatial damage distribution pattern», *Int. J. Radiat. Biol.* **88**, 103 (2012).

[34] F. Ballarini, A. Ottolenghi, «A Model of Chromosome Aberration Induction: Applications to Space Research», *Radiation Res.* **164**, 567 (2005).

[35] R.K. Sachs, D. Levy, P. Hahnfeldt, L. Hlatky, «Quantitative analysis of radiation-induced chromosome aberrations», *Cytogenet. Genome Res.* **104**, 142 (2004).

[36] A. Kowalska *et al.*, «Initial radiation DNA damage observed in prematurely condensed chromosomes of G2-phase human lymphocytes and analytical model of ion tracks», *Eur. Phys. J. D* **74**, 17 (2020).

[37] A. Kowalska *et al.*, «Production and distribution of chromosome aberrations in human lymphocytes by particle beams with different LET», *Radiat. Environ. Biophys.* **58**, 99 (2019).

[38] A. Tartas *et al.*, «Modeling of dose and linear energy transfer homogeneity in cell nuclei exposed to alpha particles under various setup conditions», *Int. J. Radiat. Biol.* **99**, 1248 (2023).

[39] B. Brzozowska, A. Tartas, A. Wojcik, «Monte Carlo Modeling of DNA Lesions and Chromosomal Aberrations Induced by Mixed Beams of Alpha Particles and X-Rays», *Front. Phys.* **8**, (2020).

[40] C. Hartel *et al.*, «Chromosomal aberrations in peripheral blood lymphocytes of prostate cancer patients treated with IMRT and carbon ions», *Radiother. Oncol.* **95**, 73 (2010).

[41] R.M. Anderson *et al.*, «Complex chromosome aberrations in peripheral blood lymphocytes as a potential biomarker of exposure to high-LET, α-particles», *Int. J. Radiat. Biol.* **76**, 31 (2000).

[42] N. Tang *et al.*, «Influence of chromatin compaction on simulated early radiation-induced DNA damage using Geant4-DNA», *Med. Phys.* **46**, 1501 (2019).